HHS Public Access

Author manuscript

Mol Cell Endocrinol. Author manuscript; available in PMC 2020 September 15.

Published in final edited form as:

Mol Cell Endocrinol. 2019 September 15; 495: 110509. doi:10.1016/j.mce.2019.110509.

Acetylation modulates thyroid hormone receptor intracellular localization and intranuclear mobility

Cyril S. Anyetei-Anum, **Rochelle M. Evans**, **Amanda M. Back**, **Vincent R. Roggero**, **Lizabeth A. Allison***

Department of Biology, College of William and Mary, 540 Landrum Drive, Integrated Science Center 3030, Williamsburg, VA 23187, U.S.A.

Abstract

The thyroid hormone receptor (TR) undergoes nucleocytoplasmic shuttling, but is primarily nuclear-localized and mediates expression of genes involved in development and homeostasis. Given the proximity of TR acetylation and sumoylation sites to nuclear localization (NLS) and nuclear export signals, we investigated their role in regulating intracellular localization. The nuclear/cytosolic fluorescence ratio (N/C) of fluorescent protein-tagged acetylation mimic, nonacetylation mimic, and sumoylation-deficient TR was quantified in transfected mammalian cells. While nonacetylation mimic and sumoylation-deficient TRs displayed wild-type N/C, the acetylation mimic's N/C was significantly lower. Importins that interact with wild-type TR also interact with acetylation and nonacetylation mimics, suggesting factors other than reduced importin binding alter nuclear localization. FRAP analysis showed wild-type intranuclear dynamics of acetylation mimic and sumoylation-deficient TRs, whereas the nonacetylation mimic had significantly reduced mobility and transcriptional activity. Acetyltransferase CBP/p300 inhibition enhanced TR's nuclear localization, further suggesting that nonacetylation correlates with nuclear retention, while acetylation promotes cytosolic localization.

Keywords

acetylation; fluorescence recovery after photobleaching (FRAP); nuclear receptor; nuclear localization; sumoylation; thyroid hormone; thyroid hormone receptor

1. Introduction

The thyroid hormone receptor (TR) belongs to a large, evolutionarily conserved superfamily of nuclear receptors that function as ligand-regulated transcriptional activators or repressors.

*Corresponding author. laalli@wm.edu (L.A. Allison).

Conflicts of interest

The authors declare that there is no conflict of interest that could be perceived as prejudicing the impartiality of the research reported.

Appendix A. Supplementary data

Supplementary data to this article can be found online.

The major subtypes of TR, TRα1 and TRβ1, regulate the activity of numerous thyroid hormone-dependent physiological and developmental processes, including metabolism, cellular growth, and cell proliferation (Anyetei-Anum et al., 2018; Mullur et al., 2014). The functional capacity of TR as a transcription factor depends, in part, on its nucleocytoplasmic shuttling (Bunn et al., 2001). Our prior studies show that nuclear entry of TRα1, through nuclear pore complexes, is mediated by interactions with the nuclear transport factors importin 7, importin β1, and adapter importin al. Importin binding occurs at lysine and arginine-rich nuclear localization signal (NLS) motifs termed NLS-1 and NLS-2 that reside in the hinge and A/B domains of TR, respectively (Mavinakere et al., 2012; Roggero et al., 2016). Notably, TRβ1 lacks NLS-2 in the A/B domain, and tends to have a slightly more cytosolic localization than TRα1 at steady-state (Anyetei-Anum et al., 2018). Exit of TR from the nucleus is mediated by multiple exportins and nuclear export signal (NES) motifs in the ligand-binding domain (LBD), including a motif spanning helices 3 to 6 (NES-H3/H6) and another in helix 12 (NES-H12) (Grespin et al., 2008; Mavinakere et al., 2012; Subramanian et al., 2015). The fine balance between nuclear import and nuclear export of TR is emerging as a central control point for regulation of hormone-responsive gene expression (Zhang et al., 2018). The question is thus raised of whether post-translational modification (PTM) contributes to this fine balance, by altering the contact frequency of TR with the transport machinery and nuclear factors, such as DNA response elements and transcriptional coregulators that promote nuclear retention.

Post-translational modifications extend the functional capacity of amino acids through modulation of the structure and function of many proteins, including altering enzymatic activity, transcriptional activity, stability or degradation, subcellular localization, protein-protein interactions, and diverse cell signaling pathways (Abdel-Hafiz and Horwitz, 2014; Anderson et al., 2012; Becares et al., 2017; Csizmok and Forman-Kay, 2018; Cui et al., 2016; Faresse, 2014; Rothenbusch et al., 2012; Soutoglou et al., 2000; Thomas et al., 2004; Wang et al., 2011). Concordantly, TR undergoes PTMs that influence its functional activities. For example, ubiquitination of liganded TR is known to target the receptor for rapid proteasome-mediated degradation (Bondzi et al., 2011; Brunelle et al., 2011; Dace et al., 2000; Kenessey and Ojamaa, 2005; Wadosky et al., 2016); and phosphorylation regulates DNA binding and transcriptional activation, and may enhance nuclear retention (Liu and Brent, 2018a; Martin et al., 2014; Nicoll et al., 2003).

One of the most frequently post-translationally modified residues is lysine (Azevedo and Saiardi, 2016), which is targeted by various PTMs, including acetylation (Ali et al., 2018; Drazic et al., 2016) and sumoylation (Rodriguez, 2014), sumoylation being the addition of the small ubiquitin-like modifier (SUMO). Acetylation sites that are important for TR's transcriptional activity have been identified in the hinge domain (Lin et al., 2005; Sanchez-Pacheco et al., 2009), which also houses NLS-1 (Mavinakere et al., 2012). Further analysis demonstrated that the acetyltransferase CBP/p300 acts on both TRα1 (Sanchez-Pacheco et al., 2009) and TRβ1 (Lin et al., 2005). In addition SIRT1, a member of the sirtuin family of deacetylases, has been shown to act on TRβ1 (Suh et al., 2013). Adding to the repertoire of PTMs in TR, several studies have provided evidence that sumoylation of TR plays an essential role in fine-tuning thyroid hormone-responsive gene expression. Sumoylation sites have been identified in the DNA-binding domain (DBD) and LBD of TR (Liu and Brent,

2018b; Liu et al., 2012; Weitzel, 2016), in proximity to NES-H3/H6 and NES-H12. Although sumoylation is involved in the recruitment of various cofactors to thyroid hormone response elements (TREs) for transcriptional repression or activation, the role sumoylation plays in nuclear localization of human TR had not been investigated.

Given the proximity of PTMs to NES and NLS motifs in TR, we thus sought to determine the role of lysine acetylation and sumoylation in modulating the intracellular localization and intranuclear dynamics of TRα1 and TRβ1.

2. Materials and methods

2.1 Plasmids

pGFP-TRα1 encodes functional, N-terminal GFP-tagged human TRα1; and pGFP-TRβ1 encodes functional, N-terminal GFP-tagged human TRβ1 (Mavinakere et al., 2012). pmCherry-TRα1 and pmCherry-TRβ1 encode functional, N-terminal red fluorescent protein (mCherry)-tagged human TR fusion proteins. cDNAs for the TRα1 and TRβ1 sumoylation-deficient mutant (lysine to glutamine substitutions), acetylation mimic (lysine to glutamine substitutions), and nonacetylation mimic (lysine to arginine substitutions) were synthesized by Invitrogen GeneArt Gene Synthesis (ThermoFisher Scientific), and subcloned into EGFP-C1 and mCherry-C1 vectors (N-terminal tag, Clontech Laboratories, Inc.). Constructs were verified by DNA sequencing. 2xDR4-SV40-Luc consists of two copies of a positive, direct repeat TRE (DR+4) in the firefly luciferase vector pGL3 (Roggero et al., 2016). The plasmid pGL4.74 encodes *Renilla* luciferase (Promega).

2.2. Cell culture and transient transfection

HeLa cells (American Type Culture Collection [ATCC], # CCL-2; human cervical adenocarcinoma) and HepG2 cells (ATCC #HB-8065; human hepatocellular carcinoma) were cultured in Minimum Essential Medium (MEM) supplemented with 10% fetal bovine serum (FBS) (Life Technologies) at 37°C under 5% CO_2 and 98% humidity. GH4C1 cells (ATCC # CCL-82.2, rat pituitary tumor) were cultured in Ham's F10 medium supplemented with 15% horse serum and 2.5% FBS. Cells were seeded in 6 well culture dishes at a density of ~ 2-3 × 10^5 cells per well on 22 mm glass coverslips (Thermo Fisher Scientific) for HeLa and HepG2 cells, or German glass coverslips with poly-D-lysine coating (Neuvitro Corporation) for GHFC1 cells. Twenty-four hours post-seeding cells were transfected with the desired expression plasmids using Lipofectamine 2000 (Life Technologies), according to the manufacturer's recommendations. Approximately 24 h post-transfection, cells were fixed in 3.7% formaldehyde, and coverslips were mounted with Fluoro-Gel II mounting medium (Electron Microscopy Sciences) containing the DNA counter stain 4′,6-diamidino-2′-phenylindole dihydrochloride (DAPI, 0.5μg/ml). Cells were then analyzed for the cellular localization of GFP or mCherry-TRα1/TRβ1 or acetylation/nonacetylation mimics by fluorescence microscopy. In the pharmacological inhibition experiments, cells were treated with the CBP/p300-specific inhibitor C646 (4-24 μM, MilliporeSigma) (Bowers et al., 2010; Gao et al., 2013) and the general deacetylase inhibitor Trichostatin A (TSA) (4 nM, MilliporeSigma) (Bondzi et al., 2011; Cui et al., 2016), for approximately 18 hours. For hormone treatments, 8 h post-transfection, transfection mixtures were replaced with 10%

charcoal-stripped FBS (Gibco) containing MEM, supplemented with varying amounts of 3,3′,5-triiodo-L-thyronine (T3, MilliporeSigma) from 0 to 100 nM (Bunn et al., 2001).

2.3. Analysis of nucleocytoplasmic distribution

An inverted Nikon ECLIPSE TE2000-E fluorescence microscope (Nikon Ultraviolet Excitation: UV-2E/C filter block for DAPI visualization; Blue Excitation: B-2E/C filter block for GFP visualization; Red Excitation: T-2E/C filter block for mCherry visualization) was used with a Nikon Plan Apo 40x/0.75 objective. A CoolSNAP HQ2 CCD camera (Photometries) and NIS-Elements AR software (Nikon) was used for image acquisition, primary image processing, and quantitative analysis. Slides were blinded by members of the lab to ensure scoring was performed without knowledge of treatment. A region of interest (ROI) was positioned inside both the nucleus and cytosol of cells and fluorescence intensity was recorded for each, with a minimum of three biological replicates and 100 ROI-analyzed cells per replicate. Nuclear to cytosolic fluorescence ratios (N/C) ratios were quantified using Nikon NIS Elements software and transferred to Microsoft Excel to be normalized to baseline conditions for corresponding biological replicates, with N/C set to 1.0 for wild-type TR nuclear localization. A normalized N/C value greater than 1.0 indicates a more nuclear distribution than wild-type TR under baseline conditions, while a normalized N/C value less than 1.0 indicates a more cytosolic distribution than wild-type TR under baseline conditions.

2.4. Fluorescence recovery after photobleaching (FRAP)

Twenty-six hours post-transfection, HeLa cells were washed with Dulbecco's phosphate buffered saline (D-PBS). Cells were then incubated MEM-α medium (nucleosides, no phenol red) for the duration of the assay. After the addition of MEM-α, plates were incubated in an OkoLab Incubation System (Warner Instruments, Inc.) which maintained conditions at 37°C and 5% CO_2. A Nikon A1Rsi confocal microscope Ti-E-PFS (Nikon Inc.) with a 60x oil objective was used for all FRAP experiments. The 488-nm line of krypton-argon laser with a band-pass of 525/50 nm emission filter was used for GFP detection. A solid-state 405-nm line of laser with a band-pass of 450/50 emission filter was used exclusively for photobleaching. The "Perfect Focus System" (PFS) was applied during the duration of the experiments. Both acquisition and photobleaching were coordinated within NIS-Elements AR (Nikon). Using the stimulation module of NIS-Elements, the total experimental time for the assay was approximately 35 seconds (s). The time was divided into a 5 s "pre-bleach" acquisition phase at ~2-3% laser power, 1 s of photobleaching at 100% laser power, and a post-bleach acquisition phase at ~2-3% laser power. All image acquisition was conducted through resonant scanning. Data from at least three biological independent replicates of 20 nuclei (or cytoplasm with the exclusion of nuclei) from separate cells were recorded. FRAP data were normalized from the values 0 – 1.0, where 0 was the lowest relative fluorescent intensity directly after the photobleaching phase, and 1.0 was the highest relative fluorescent intensity during post-bleach recovery. Normalized data were then used to calculate the rate of recovery; the estimated half-time value, i.e. the time required for half of the total fluorescence to recover back into the bleached region; and the mobile and immobile fractions.

2.5. Luciferase reporter gene assay

HeLa cells were seeded at 2.0×10^4 cells per well in a white 96-well plate (PerkinElmer). Twenty four hours after seeding, cells were transiently transfected with expression plasmids for GFP-TRα1 wild-type or nonacetylation and acetylation mimics, TRE (DR+4)-firefly luciferase reporter or empty vector (no TRE), and *Renilla* luciferase internal control. Five hours post-transfection, medium was replaced with MEM containing 10% charcoal-stripped FBS (Life Technologies), supplemented or not with 100 nM T3. After an additional 19 h, a Dual-Glo® Luciferase Assay (Promega) was performed, according to the manufacturer's protocol. Four independent, biologically separate replicate experiments were performed, with 8 wells assayed per treatment.

2.6. GFP-Trap®_A coimmunoprecipitation and immunoblotting

HeLa cells were seeded in 100 mm vented plates at a concentration of 11×10^5 cells per plate in MEM supplemented with 10% FBS. Twenty-four hours post-seeding, each plate was transfected with the desired expression plasmids using Lipofectamine 2000. After 26 h, GFP-Trap®_A (Chromotek) coimmunoprecipitation assays were performed as described (Roggero et al., 2016). Samples of unbound and bound proteins were analyzed by immunoblotting. Membranes were stained for total protein with Ponceau S solution (MilliporeSigma), quantified by scanning densitometry using NIH ImageJ software, then destained prior to application of antibodies at the following concentrations: anti-GFP (Santa Cruz), 1:2000; anti-importin 7 (Abcam), 1:1000; anti-importin (karyopherin) β1 (Santa Cruz), 1:1000; anti-importin α1 (Abcam), 1:1000; horseradish peroxidase (HRP)-conjugated donkey anti-rabbit IgG (GE Healthcare Life Sciences); or HRP-sheep anti-mouse IgG (Santa Cruz). Protein size was confirmed using Pre-Stained Kaleidoscope Protein Standards (Bio-Rad). X-ray films were quantified by scanning densitometry using NIH ImageJ software.

2.7. Statistical analysis

All data are expressed as mean ± SEM. A student's t-test was used to calculate *P* values. All *P* values were two-tailed, and $P < 0.05$ was considered statistically significant.

3. Results

3.1. Acetylation alters TRα1 and TRβ1 intracellular localization

Acetylation sites have been previously characterized at lysine (K) 130, 134, and 136 in TRα1 (numbered as K128, 132, and 134 in [Sanchez-Pacheco et al., 2009]). TRβ1 has been shown to be acetylated but the specific residues were not identified (Lin et al., 2005); however, the three lysine acetylation sites in TRα1 are conserved between TRα1 and TRβ1, corresponding to K184, 188, and 190 in TRβ1 (Fig. 1A). Of interest, these acetylation sites occur in the hinge domain, within the well-characterized classical bipartite NLS-1 of TRα1 (^{130}**K**RVA**K**R**K**LIEQNRERRRK^{147}) and TRβ1 (^{184}**K**RLA**K**R**K**LIEENREKRRR^{201}) (Mavinakere et al., 2012). To examine whether acetylation plays a role in TR's intracellular localization, we introduced three point mutations into TRα1 and TRβ1 at these acetylation sites, in which lysines were substituted with either glutamine (Q) or arginine (R). Because acetylation of positively-charged lysine both reduces its charge and increases its polarity,

changing acetyl-K sites to a polar Q or a positively-charged R mimics the acetylated or nonacetylated state, respectively (DePaolo et al., 2016; Sanchez-Pacheco et al., 2009).

Here, we use our standard, validated approach of transient transfection assays in HeLa (human) cells to compare distribution patterns of fluorescent protein-tagged wild-type and mutant TRs. Our prior studies have demonstrated that in HeLa cells, which do not express detectable levels of TRα1 and TRβ1, overexpression of wild-type TR does not saturate the capacity of the nuclear import machinery, does not lead to non-specific protein aggregation, nor do fluorescent protein tags alter localization patterns. Further, wild-type TR is primarily nuclear over a wide range of expression levels in transfected cells (Anyetei-Anum et al., 2018; Bonamy et al., 2005; Bondzi et al., 2011; Bunn et al., 2001; Roggero et al., 2016). After transient transfection of TR expression plasmids into HeLa cells, the intracellular distribution patterns of mCherry-TRα1-nonacetylation mimic (K130/134/136R) and mCherry-TRα1-acetylation mimic (K130/134/136Q) were compared to wild-type TRα1 using quantitative fluorescence microscopy. Strikingly, the mCherry-TRα1-acetylation mimic had a significantly increased cytosolic localization compared to wild-type TRα1 (Fig. 1B, C; normalized N/C of approximately 0.60; $P = 0.0012$). In contrast, the nonacetylation mimic was not significantly different from wild-type (normalized N/C of approximately 1.0; $P = 0.4784$). The experiments described were performed under standard culture conditions (MEM/10% FBS), with undefined hormone levels. When we performed experiments using MEM/10% charcoal-stripped FBS in the absence of thyroid hormone (T3), or in the presence of 100 nM T3, we observed no significant difference in localization patterns of wild-type TRα1 or of the acetylation and nonacetylation mimics (data not shown). These findings are consistent with our prior studies which have shown that the intracellular localization of wild-type TRα1 is not sensitive to T3 (Bonamy et al., 2005; Bunn et al., 2001) (see also Fig. 8B of this report). Given the ligand-independence of TRα1 localization patterns, subsequent experiments were performed under standard culture conditions (MEM/10% FBS), unless otherwise indicated.

We next analyzed the intracellular distribution patterns of the GFP-TRβ1-nonacetylation mimic (K184/188/190R), and the GFP-TRβ1-acetylation mimic (K184/188/190Q). Comparable to results for TRα1, we observed a shift towards a significantly more cytosolic localization of the TRβ1-acetylation mimic (Fig. 1D, E; normalized N/C of approximately 0.20; $P < 0.0001$). The TRβ1 nonacetylation mimic also showed a significant, albeit less marked, shift towards the cytosol compared to wild-type TRβ1 (normalized N/C of approximately 0.80; $P = 0.05$). The slight increase in cytosolic localization is likely not significant at the cellular level, particularly given that the nonacetylation mimic was 4-fold more nuclear-localized than the acetylation mimic ($P = 0.003$). These data suggest that TRβ1 shuttling is more sensitive to changes from K to R residues in NLS-1 than TRα1, since TRβ1 relies solely upon this NLS for its nuclear entry (see Fig. 1A).

To confirm that these observations are not specific to HeLa cells, we also analyzed the distribution of the acetylation and nonacetylation mimics in two additional cell lines that express endogenous TRs: HepG2 (hepatocellular carcinoma) cells that express low levels of TRα1 and TRβ1, and GH4C1 (rat pituitary tumor) cells that express high levels of both TRα1 and TRβ1. Comparable to the cytosolic shift observed in HeLa cells, in HepG2 cells

(Fig. S1) and GH4C1 cells (Fig. S2), we also observed a shift toward a more cytosolic localization of the TRα1 and TRβ1-acetylation mimics, relative to wild-type and the nonacetylation mimics.

Overall, these results provide evidence that modification of lysines in NLS-1 of TRα1 and TRβ1 alters the fine balance of nucleocytoplasmic shuttling, possibly by inhibiting nuclear import or facilitating nuclear export.

3.2. Importin 7, importin β1, and importin α1 interact with TR acetylation mimics

Our prior study showed that importin β1 and the adapter importin α1 interact with both NLS-1 and NLS-2, while importin 7 likely only interacts with NLS-2 in TRα1 (Roggero et al., 2016). In contrast, nuclear entry of TRβ1 is facilitated only by the importin α1/β1 heterodimer interacting with NLS-1. Since we showed here that TRα1 and TRβ1-acetylation mimics have a significant cytosolic population, we sought to determine whether their shift in intracellular distribution was due to impaired binding with the importins, due to acetylation neutralizing the positive charge on lysine. To this end, we performed “GFP-trap” coimmunoprecipitation assays on lysates from HeLa cells that had been transfected with expression plasmids for GFP, GFP-TRα1, GFP-TRα1-acetylation (K to Q) or nonacetylation mimics (K to R); and GFP-TRβ1, GFP-TRβ1-acetylation or nonacetylation mimics (Fig. 2).

First, we confirmed that the aforementioned fusion proteins were all successfully expressed in the transfected HeLa cells and immunoprecipitated by the GFP-trap assay. Western blot analysis of immunoprecipitated samples with anti-GFP antibodies demonstrated the presence of wild-type TR and the acetylation and nonacetylation mimics (Fig. 2A). Next, samples of unbound proteins (immunosupernatant) and bound proteins (immunoprecipitates) were analyzed for the presence of importins α1, β1, and 7 on separate blots using importin-specific antibodies. Endogenous importin α1, importin β1, and importin 7 were successfully coimmunoprecipitated (trapped) with GFP-TRα1, GFP-TRα1-acetylation mimic, and the GFP-TRα1-nonacetylation mimic, but not with GFP alone (Fig. 2B). Likewise, importin α1 and importin β1 were trapped with GFP-TRβ1, GFP-TRβ1-acetylation mimic, and the GFP-TRβ1-nonacetylation mimic, but not with GFP alone (Fig. 2C). As expected, importin 7 was not coimmunoprecipitated with any of the TRβ1 variants, since they all lack NLS-2.

The relative amount of binding between wild-type TR, the acetylation and nonacetylation mimics, and importins was measured by densitometry analysis (Fig. 2D). The binding of importins to the TRα1 and TRβ1-nonacetylation mimics was not significantly different from wild-type binding ($P > 0.200$). Further, there was no significant change in binding of wild-type TRα1 or the acetylation mimic to importin 7 ($P = 0.694$) or to importin β1 ($P = 0.273$); however, the GFP-TRα1-acetylation mimic showed a significant increase in binding to the adaptor importin α1 ($P = 0.046$). Interestingly, there was a significant increase in the relative binding of TRβ1 to importin β1 ($P = 0.033$), although there was no significant change in binding of GFP-TRβ1 and the acetylation mimic to the adaptor importin α1 ($P = 0.133$). It is possible that the increases seen in importin α1 binding to the GFP-TRα1-acetylation mimic, and importin β1 (indirectly binding via the adaptor importin a1) to the GFP-TRβ1-acetylation mimic are due to conformational changes that differentially impact formation or

stability of the importin α1/β1 heterodimer. Taken together, these data suggest that although TR acetylation status does not have a major impact on interactions with importins α1, β1, and 7 *in vivo,* acetylation does enhance interaction of TR with components of the importin α1/β1 heterodimer.

3.3. TRα1 and TRβ1 nonacetylation mimics have altered intranuclear mobility profiles

Having shown that the K to Q acetylation mimics of TRα1 and TRβ1 display a dramatic shift in localization to the cytoplasm that is not due to reduced importin binding, the question still remained of whether other pathways could explain their altered intracellular distribution patterns. The hinge region falls between the DBD and LBD of TR (Fig. 1A) and, in addition to harboring NLS-1, also contributes to DNA binding, activation function, ligand binding, and corepressor interactions (Mondal et al., 2016; Nascimento et al., 2006; Pawlak et al., 2012; Zhang, 2017). We thus hypothesized that the acetylation state of TR may act to alter TR's intranuclear mobility profile. Previously, we used fluorescence recovery after photobleaching (FRAP) to examine nucleocytoplasmic shuttling dynamics of TR (Grespin et al., 2008; Subramanian et al., 2015). Here, to analyze intranuclear mobility, we used a variation of FRAP, termed strip-FRAP (Weiss, 2004; Yang et al., 2010). Strip-FRAP was selected as the method of choice based on the smooth distribution of TR in the nucleus (e.g. see Fig. 1B, D). In this method, a small strip through the nucleus is photobleached and mobility is monitored by the recovery of fluorescent proteins into the bleached strip.

As shown in Fig. 3, wild-type TRα1 is highly dynamic in its intranuclear mobility; the calculated half-maximal recovery time (t½) ranged from approximately 0.6 to 0.7 s, with 99% of TRα1 within the mobile fraction (Table 1). When we compared the intranuclear FRAP profile of the corresponding nonacetylation or acetylation mimics, data revealed an altered intranuclear mobility profile for the nonacetylation mimic. There was a statistically significant difference in the recovery rate, and percentage of the nonacetylation mimic in the mobile and immobile fractions compared with wild-type (Fig. 3A, B; Table 1). On average, t½ for the nonacetylation mimic was 1.01 s with 95% of TR in the mobile fraction (Fig. 3A, B). In contrast, the TRα1 acetylation mimic showed an intranuclear mobility profile comparable to wild-type, with the exception that the half-time slope was altered (Fig. 3A, C; Table 1). On average, t½ for the acetylation mimic was 0.6 s, with 99% in the mobile fraction.

We then analyzed cells expressing GFP-TRβ1 or the corresponding nonacetylation or acetylation mimics (Fig. 4). The GFP-TRβ1-nonacetylation mimic also showed an altered intranuclear mobility profile compared to wild-type GFP-TRβ1. There was a statistically significant difference in the recovery rate, mobile and immobile fractions, half-time slope, and t½ of the TRβ1-nonacetylation mimic compared with wild-type (Fig. 4A, B; Table 1). On average, t½ for the nonacetylation mimic was 1.8 s with 90% in the mobile fraction, compared with a t½ of 0.8 s for the wild-type, with 98% in the mobile fraction. In contrast, the GFP-TRβ1-acetylation mimic's intranuclear mobility profile was comparable to the wild-type, with the exception that the recovery rate (slope) was slightly altered (Fig. 4A, C; Table 1).

Finally, to determine whether there were any differences in mobility parameters between cellular compartments that might explain the more cytosolic localization of acetylation mimics, we compared the mobility of the GFP-TRβ1-acetylation mimic in the cytosol to that of cytosolic wild-type GFP-TRβ1. We found that the cytosolic mobilities were comparable, suggesting that the cytosolic shift of the acetylation mimic is due to factors other than reduced cytosolic mobility (Fig. 4D, E; Table 1).

3.4. TRα1 and TRβ1 nonacetylation mimics undergo intranuclear rearrangement

While quantifying the intranuclear FRAP profiles of TR variants by confocal microscopy, we also qualitatively examined their distribution patterns within the nucleus. In nuclei expressing wild-type TR or the acetylation or nonacetylation mimics, TR was always excluded from nucleoli (Fig. 5, dark ovals). Notably, in addition, the GFP-TRα1 and GFP-TRβ1 nonacetylation mimics both displayed remarkably altered patterns of intranuclear rearrangement. In approximately 85% of cells analyzed (n=60), there was a marked shift from the characteristic diffuse, smooth pattern of wild-type TRα1 (Fig. 5A) and TRβ1 (Fig. 5C), to a granular, mottled appearance of the nonacetylation mimics (Fig. 5B, D). These observations suggest the possibility that TRα1 and TRβ1 nonacetylation mimics interact with greater contact frequency with insoluble nuclear factors that reduce their intranuclear mobility.

3.5. Acetylation and nonacetylation mimics alter ligand-dependent transcriptional activity

We next sought to ascertain whether changes in nuclear localization and intranuclear dynamics of the acetylation and nonacetylation mimics, respectively, impact TR-mediated gene expression. A firefly luciferase reporter gene under the positive control of a thyroid hormone response element (TRE) was used to examine ligand-dependent transactivation by wild-type TR and the nonacetylation and acetylation mimics. As expected, TRα1 and TRβ1 induced luciferase reporter activity in the presence of T3; on average, there was a 4-fold increase in relative luciferase activity (Fig. 6). In contrast, on average, the nonacetylation mutants showed a diminished response to T3, relative to the wild-type and acetylation mimics, with either little or no induction. Relative luciferase activity of the TRα1 and TRβ1 acetylation mimics was greater than the nonacetylation mimics, with a particularly robust response from the TRβ1 acetylation mimic which, on average, showed over a 5-fold increase in reporter gene activity in the presence of T3 (Fig. 6B). Given the correlation between reduced intranuclear mobility and impaired ligand-dependent transcriptional activity, these findings suggest that receptor intranuclear dynamics are of more importance than cytosolic localization in determining transcriptional output.

3.6. Inhibition of the acetyltransferase CBP/p300 promotes TRβ1 nuclear retention

The altered intranuclear dynamics of the TR nonacetylation mimics suggest that acetylation may act as a regulatory switch for TRα1 or TRβ1 release from DNA response elements or other coregulators of transcription. To begin to explore this model, we sought to ascertain whether acetylation occurs within the nucleus. To this end, we examined the effect of inhibiting the acetyltransferase CBP/p300, which is localized to the nucleus, using the specific inhibitor, C646 (Bowers et al., 2010; Gao et al., 2013) (Fig. 7). Since TRβ1 typically has a small cytosolic population at steady-state (Mavinakere et al., 2012), we

primarily focused on TRβ1 in these studies to allow greater visualization of any increased nuclear localization. We predicted that if CBP/p300 is responsible for acetylating TRβ1 in the nucleus, then inhibiting this acetyltransferase would lead to more unacetylated TRβ1 and a more nuclear population. As predicted, pharmacological inhibition of CBP/p300 by C646 in GFP-TRβ1-expressing HeLa cells caused a dose-dependent increase in TRβ1‘s nuclear localization, with the normalized N/C significantly different from wild-type at concentrations ranging from 8 to 24 μM C646 ($P = 0.0008$) (Fig. 7A, C). At higher C646 exposure levels, cell viability decreased. These data provide further support for a model in which deacetylation of TR promotes nuclear retention.

We also examined the effects of trichostatin A (TSA), a general deacetylase inhibitor (Cui et al., 2016), on receptor localization. Exposure to TSA caused a significant increase in nuclear localization (normalized N/C of approximately 1.4) of both mCherry-tagged and GFP-tagged TRβ1 ($P = 0.0447$ and $P = 0.0114$, respectively) (Fig. 7B, C). We had anticipated that by globally blocking deacetylation, the population of acetylated TR would increase, leading to a more cytosolic distribution. However, a likely reason for the increase in nuclear retention of TRβ1 under these conditions is because of TSA-induced histone acetylation (Xu et al., 2018) and concomitant increased availability of TREs in the newly exposed DNA. Similarly, a prior study showed that TSA treatment of HeLa cells increased the nuclear localization of GFP-class II transactivator (CIITA) (Spilianakis et al., 2000). CBP/p300 also has histones as a target, so inhibition of this acetyltransferase would inhibit acetylation of both histones and TRβ1. In this case, we propose that the impact on receptor localization comes through maintenance of TRβ1 in a nuclear, nonacetylated state regardless of chromatin being in a more closed state. On the flip side, when deacetylases are inhibited by TSA, we propose that the driver of localization is the increased access to chromatin, despite the maintenance of TR in an acetylated state.

To further explore the impact of specifically inhibiting the CBP/p300 acetylase and inhibiting deacetylation, in general, we also assessed the impact of C646 and TSA on the intracellular distribution patterns of the TRβ1 acetylation and nonacetylation mimics (Fig. 7C). We predicted that the acetylation mimic would maintain its more cytosolic distribution, and the nonacetylation mimic would maintain its more nuclear distribution, since although mimicking acetylation and nonacetylation, respectively, the changes from K→Q and K→R in these mutants do not provide substrates for either acetylation or deacetylation. As anticipated, neither inhibition of the CBP/p300 acetylase by C646, nor general inhibition of deacetylases by TSA had an observable effect on the distribution of the acetylation and nonacetylation mimics.

3.7. Sumoylation of TR does not affect nuclear localization

Sumoylation sites have been previously identified at positions K283 and K389 in NES-H3/H6 of TRα1; and at K50 in the A/B domain, K146 in the DBD, and K443 near NES-H12 and the AF-2 transactivation region of TRβ1 (Liu et al., 2012) (Fig. 8A). To determine whether sumoylation of lysine residues plays a regulatory role in nuclear localization of TR, expression plasmids were constructed that encode GFP-tagged mutants of TRα1 and TRβ1 that are unable to be sumoylated, by substituting K for Q at the well-characterized

sumoylation sites (Fig. 8A). After transient transfection into HeLa cells, the intracellular distribution patterns of the sumoylation-deficient fusion proteins were compared to wild-type GFP-TRα1 and GFP-TRβ1 using quantitative fluorescence microscopy. N/C was normalized to wild-type TR under standard culture conditions (MEM/10% FBS).

There was no significant difference in the intracellular distribution patterns of sumoylation-deficient mutant TRα1 (K283/389Q), compared with wild-type TRα1. On average, the normalized N/C of the SUMO mutant was approximately 1.0, either under standard culture conditions (MEM/10% FBS) or in MEM supplemented with charcoal-stripped FBS, in the presence or absence of thyroid hormone (T3) (Fig. 8B; $P > 0.05$). Similarly, there was no significant difference in intracellular distribution patterns between wild-type TRβ1 and the sumoylation-deficient mutant TRβ1 (K50/146/443Q). On average, the normalized N/C of the SUMO mutant was approximately 1.0, either under standard culture conditions (MEM/10% FBS), or in MEM supplemented with charcoal-stripped FBS in the presence of T3 (Fig. 8C; $P > 0.05$). However, there was a statistically significant difference in normalized N/C between wild-type TRβ1 and sumoylation-deficient TRβ1 in the absence of T3 ($P = 0.009$). This difference in distribution patterns is explained by the corresponding statistically significant difference between wild-type TRβ1 in the absence of T3 and under standard culture conditions ($P = 0.016$). In the absence of T3, wild-type TRβ1 showed an increase in cytosolic localization (normalized N/C of approximately 0.8) relative to standard culture conditions, whereas the SUMO mutant retained a normalized N/C of approximately 1.0. Given that these changes in distribution pattern are quite small they likely are not significant at the cellular level. Although 100 nM T3 is a standard amount used in cultured cells (Bunn et al., 2001), it is considered above physiological levels of T3. To determine whether ligand-dependent effects on nuclear localization would be observed at lower doses, we tested a range of T3 concentrations (0, 1, 5, 10, 50, 100 nM). There were no observable differences in localization patterns for wild type or the sumoylation-deficient mutant over this range of concentrations (Fig. S3).

Finally, to assess whether sumoylation plays a role in modulating the intranuclear dynamics of TR, we performed intranuclear strip-FRAP on HeLa cells expressing wild-type or sumoylation-deficient TRα1 and TRβ1. The intranuclear FRAP profiles of both sumoylation-deficient TRα1 (Fig. 8D) and TRβ1 (Fig. 8E) were comparable to wild-type TRs; there was no significant difference in their recovery rate, mobile and immobile fractions, half-time slope, and t½ (Table 1). Taken together, these data suggest that sumoylation does not play an important role in nuclear localization or intranuclear dynamics of TR.

4. Discussion

Our data show that K to Q substitution mutations within NLS-1 of TRα1 and TRβ1, which mimic acetylated lysine, promote cytosolic localization of TR but at the same time enhance ligand-dependent transcriptional activity, while mutants that mimic nonacetylated TR (K to R substitution) have reduced intranuclear mobility, suggesting that this reduced mobility correlates with greater nuclear retention and impaired ligand-dependent transcriptional activity. Finally, pharmacological inhibition of the acetyltransferase CBP/p300 increased

GFP-TRβ1's nuclear localization in a dose-dependent manner, suggesting that acetylation occurs within the nucleus. In contrast, a sumoylation-deficient TR had a comparable intracellular distribution pattern and intranuclear profile to wild-type TR. This pattern is consistent with the findings of a recent study that focused on sumoylation sites in chicken TRα, observing that a sumoylation-defective mutant had wild-type subcellular localization [reported as data not shown in (Weitzel, 2016)]. Taken together, our data provide support for a model in which local conformational changes within NLS-1, induced by acetylation, may act as a potential regulatory mechanism for fine-tuning T3-induced gene expression. In its nonacetylated state, TR would be bound to transcriptional corepressors and heterodimerization partners, reducing its intranuclear mobility. When TR is acetylated by the transcriptional coactivator CBP/p300 it would then have increased intranuclear mobility and would become more accessible to the nuclear export machinery. SIRT1 is known to deacetylate TRβ1, potentially leading to ubiquitin-mediated degradation (Suh et al., 2013); however, the deacetylase that acts on TRα1, and the cellular compartment in which deacetylation of TR occurs are unknown.

Several lines of evidence lend support to this model in which acetylation acts as a regulatory switch for nuclear retention and transcriptional output. A previous study showed that the TRα1-nonacetylation mimic has increased binding to TREs *in vitro,* but is unable to recruit transcriptional coactivators, and is not able to mediate T3-dependent transactivation in a luciferase reporter gene assay (Sanchez-Pacheco et al., 2009). In this study, however, the authors did not examine the TRα1 acetylation mimic (Sanchez-Pacheco et al., 2009). In addition, the observed granular distribution of the TR nonacetylation mutants shown in the present study is reminiscent of ligand-induced intranuclear reorganization of GFP-estrogen receptor α (ERα) and GFP-retinoic acid receptor β (Maruvada et al., 2003), CFP-ERα (Tanida et al., 2015) and YFP-tagged glucocorticoid receptor (GR) (Schaaf et al., 2006), indicating transcriptional activity. The pattern is also comparable to the intranuclear rearrangement observed for GFP-TRβ1 in HeLa cells in response to ligand (Baumann et al., 2001). Our finding of intranuclear reorganization suggests the possibility that TRα1- and TRβ1-nonacetylation mimics may interact with other nuclear receptors, chromatin, or insoluble nuclear factors to reduce their intranuclear mobility. Further support for our model is that intranuclear mobility and reorganization of the NF-κB (nuclear factor kappa-light-chain-enhancer of activated B cells) subunit p65 is determined by its affinity for specific DNA sequences (Schaaf et al., 2006), while mobility of GR is decreased by ligand-dependent targeting of the receptor to specific subdomains within the nucleus (Schaaf et al., 2005).

The role of acetylation in the intracellular localization of transcription factors is not without precedent. CBP/p300 acetylates thousands of sites and, typically in response to ligand, targets a number of nuclear receptors, by a "hit and run" mechanism, including the androgen receptor (Thomas et al., 2004), ER (Cui et al., 2004; Wang et al., 2001), the farnesoid X receptor (Kemper et al., 2009), steroidogenic factor 1 (SF-1) (Chen et al., 2005), retinoid X receptor (Zhao et al., 2007), TRβ1 (Lin et al., 2005), and TRα1 (Sanchez-Pacheco et al., 2009). The functional role of acetylation in inhibiting or promoting nuclear import is transcription factor-specific (Soniat et al., 2016). As examples, acetylation of histones H3 and H4 decreases interaction with several members of the karyopherin-β family of importins

(Soniat et al., 2016), and acetylation leads to cytoplasmic localization of the Rho guanine nucleotide exchange factor Net1A (Song et al., 2015), the Signal transducer and activator of transcription 1 (STAT1) (Antunes et al., 2011), HDAC6 (Jimenez-Canino et al., 2016), and adenovirus E1A transforming protein (Madison et al., 2002). In contrast, acetylation leads to nuclear accumulation of the androgen receptor (Jimenez-Canino et al., 2016), the hepatocyte nuclear factor-4 (HNF-4) (Soutoglou et al., 2000), and GLI1 (Mirza et al., 2019).

We had anticipated that TR acetylation mimics may be unable to interact with importins, because of their altered charge; however, this was not the case. Instead, the acetylation mimics showed enhanced interaction with components of the importin α/β heterodimer. A recent report provides a possible explanation for our observations. The surface properties of cargo molecules have been shown to impact their passage rate through nuclear pore complexes more than was previously thought (Frey et al., 2018). Even for importin-cargo complexes, findings suggest that along with exposed hydrophobic patches, charged arginine residues in cargo promote translocation by conferring attraction to the phenylalanine-glycine (FG) domains above and beyond the interactions facilitated by the importin itself, while negative charges and lysines impede passage (Frey et al., 2018). Thus, while the TR acetylation mimics analyzed in the current study are still able to interact with importins, they do not behave entirely passively, and may repel FG-domains, affecting their translocation rate through the nuclear pore complexes.

The critical role of lysine acetylation in regulating transcription factor intracellular localization is apparent, and our findings suggest that acetylation promotes cytosolic accumulation of TR. Although, the exact regulatory mechanism of TR acetylation remains to be further characterized, it is noteworthy that in other cases dysregulation of lysine acetylation has been linked to cancer and other diseases (Weinert et al., 2018). Among the acetyl-lysine residues in TRα1, the mutation K136R has been associated with hepatocellular carcinoma, along with three other mutations in the receptor, serine 40 to threonine, leucine 251 to proline, and valine 390 to alanine (Lin et al., 1999), suggesting that dysregulation of TR acetylation may contribute to disease pathology. Finally, the notion of an inter-regulated network of PTM's is gaining traction. For example, a recent study proposes a mutually exclusive acetylation-sumoylation switch, in which acetylation of the pregnane X receptor is a prerequisite for its subsequent SUMO-modification (Cui et al., 2016). Following, acetylation of TR may be part of an integrated network of PTM's that coordinate both the activation and repression of T3-responsive gene expression.

Supplementary Material

Refer to Web version on PubMed Central for supplementary material.

Acknowledgments

This work was supported by Grant 2R15DK058028 from the National Institutes of Health and Grant MCB1120513 from the National Science Foundation (to L.A.A.).

References

Abdel-Hafiz HA, and Horwitz KB (2014). Post-translational modifications of the progesterone receptors. J Steroid Biochem Mol Biol 140, 80–89. [PubMed: 24333793]

Ali I, Conrad RJ, Verdin E, and Ott M (2018). Lysine Acetylation Goes Global: From Epigenetics to Metabolism and Therapeutics. Chem Rev 118, 1216–1252. [PubMed: 29405707]

Anderson DD, Eom JY, and Stover PJ (2012). Competition between sumoylation and ubiquitination of serine hydroxymethyltransferase 1 determines its nuclear localization and its accumulation in the nucleus. J Biol Chem 287, 4790–4799. [PubMed: 22194612]

Antunes F, Marg A, and Vinkemeier U (2011). STAT1 signaling is not regulated by a phosphorylation-acetylation switch. Mol Cell Biol 31, 3029–3037. [PubMed: 21576370]

Anyetei-Anum CS, Roggero VR, and Allison LA (2018). Thyroid hormone receptor localization in target tissues. J Endocrinol 237, R19–R34. [PubMed: 29440347]

Azevedo C, and Saiardi A (2016). Why always lysine? The ongoing tale of one of the most modified amino acids. Adv Biol Regul 60, 144–150. [PubMed: 26482291]

Baumann CT, Maruvada P, Hager GL, and Yen PM (2001). Nuclear Cytoplasmic Shuttling by Thyroid Hormone Receptors. J Biol Chem 276, 11237–11245. [PubMed: 11152480]

Becares N, Gage MC, and Pineda-Torra I (2017). Posttranslational Modifications of Lipid-Activated Nuclear Receptors: Focus on Metabolism. Endocrinology 158, 213–225. [PubMed: 27925773]

Bonamy GM, Guiochon-Mantel A, and Allison LA (2005). Cancer promoted by the oncoprotein v-ErbA may be due to subcellular mislocalization of nuclear receptors. Mol Endocrinol 19, 1213–1230. [PubMed: 15650025]

Bondzi C, Brunner AM, Munyikwa MR, Connor CD, Simmons AN, Stephens SL, Belt PA, Roggero VR, Mavinakere MS, Hinton SD, et al. (2011). Recruitment of the oncoprotein v-ErbA to aggresomes. Mol Cell Endocrinol 332, 196–212. [PubMed: 21075170]

Bowers EM, Yan G, Mukherjee C, Orry A, Wang L, Holbert MA, Crump NT, Hazzalin CA, Liszczak G, Yuan H, et al. (2010). Virtual ligand screening of the p300/CBP histone acetyltransferase: identification of a selective small molecule inhibitor. Chem Biol 17, 471–482. [PubMed: 20534345]

Brunelle M, Fayad T, and Langlois MF (2011). Degradation of thyroid hormone receptor β1: existence of stable and unstable forms. Thyroid 21, 311–318. [PubMed: 21323586]

Bunn CF, Neidig JA, Freidinger KE, Stankiewicz TA, Weaver BS, McGrew J, and Allison LA (2001). Nucleocytoplasmic shuttling of the thyroid hormone receptor α. Mol Endocrinol 15, 512–533. [PubMed: 11266504]

Chen WY, Juan LJ, and Chung BC (2005). SF-1 (nuclear receptor 5A1) activity is activated by cyclic AMP via p300-mediated recruitment to active foci, acetylation, and increased DNA binding. Mol Cell Biol 25, 10442–10453. [PubMed: 16287857]

Csizmok V, and Forman-Kay JD (2018). Complex regulatory mechanisms mediated by the interplay of multiple post-translational modifications. Curr Opin Struct Biol 48, 58–67. [PubMed: 29100108]

Cui W, Sun M, Zhang S, Shen X, Galeva N, Williams TD, and Staudinger JL (2016). A SUMO-acetyl switch in PXR biology. Biochim Biophys Acta 1859, 1170–1182. [PubMed: 26883953]

Cui Y, Zhang M, Pestell R, Curran EM, Welshons WV, and Fuqua SA (2004). Phosphorylation of estrogen receptor α blocks its acetylation and regulates estrogen sensitivity. Cancer Res 64, 9199–9208. [PubMed: 15604293]

Dace A, Zhao L, Park KS, Furuno T, Takamura N, Nakanishi M, West BL, Hanover JA, and Cheng S (2000). Hormone binding induces rapid proteasome-mediated degradation of thyroid hormone receptors. Proc Natl Acad Sci U S A 97, 8985–8990. [PubMed: 10908671]

DePaolo JS, Wang Z, Guo J, Zhang G, Qian C, Zhang H, Zabaleta J, and Liu W (2016). Acetylation of androgen receptor by ARD1 promotes dissociation from HSP90 complex and prostate tumorigenesis. Oncotarget 7, 71417–71428. [PubMed: 27659526]

Drazic A, Myklebust LM, Ree R, and Arnesen T (2016). The world of protein acetylation. Biochim Biophys Acta 1864, 1372–1401. [PubMed: 27296530]

Faresse N (2014). Post-translational modifications of the mineralocorticoid receptor: How to dress the receptor according to the circumstances? J Steroid Biochem Mol Biol 143, 334–342. [PubMed: 24820770]

Frey S, Rees R, Schunemann J, Ng SC, Funfgeld K, Huyton T, and Gorlich D (2018). Surface Properties Determining Passage Rates of Proteins through Nuclear Pores. Cell 174, 202–217 e209. [PubMed: 29958108]

Gao XN, Lin J, Ning QY, Gao L, Yao YS, Zhou JH, Li YH, Wang LL, and Yu L (2013). A histone acetyltransferase p300 inhibitor C646 induces cell cycle arrest and apoptosis selectively in AML1-ETO-positive AML cells. PLoS One 8, e55481. [PubMed: 23390536]

Grespin ME, Bonamy GM, Roggero VR, Cameron NG, Adam LE, Atchison AP, Fratto VM, and Allison LA (2008). Thyroid hormone receptor alpha 1 follows a cooperative CRM1/calreticulin-mediated nuclear export pathway. J Biol Chem. 283, 25576–25588. [PubMed: 18641393]

Jimenez-Canino R, Lorenzo-Diaz F, Jaisser F, Farman N, Giraldez T, and Alvarez de la Rosa D (2016). Histone Deacetylase 6-Controlled Hsp90 Acetylation Significantly Alters Mineralocorticoid Receptor Subcellular Dynamics But Not its Transcriptional Activity. Endocrinology 157, 2515–2532. [PubMed: 27100623]

Kemper JK, Xiao Z, Ponugoti B, Miao J, Fang S, Kanamaluru D, Tsang S, Wu SY, Chiang CM, and Veenstra TD (2009). FXR acetylation is normally dynamically regulated by p300 and SIRT1 but constitutively elevated in metabolic disease states. Cell Metab 10, 392–404. [PubMed: 19883617]

Kenessey A, and Ojamaa K (2005). Ligand-mediated decrease of thyroid hormone receptor-α1 in cardiomyocytes by proteosome-dependent degradation and altered mRNA stability. Am J Physiol Heart Circ Physiol 288, H813–821. [PubMed: 15498821]

Lin HY, Hopkins R, Cao HJ, Tang HY, Alexander C, Davis FB, and Davis PJ (2005). Acetylation of nuclear hormone receptor superfamily members: thyroid hormone causes acetylation of its own receptor by a mitogen-activated protein kinase-dependent mechanism. Steroids 70, 444–449. [PubMed: 15862828]

Lin KH, Shieh HY, Chen SL, and Hsu HC (1999). Expression of mutant thyroid hormone nuclear receptors in human hepatocellular carcinoma cells. Mol Carcinog 26, 53–61. [PubMed: 10487522]

Liu YY, and Brent GA (2018a). Posttranslational Modification of Thyroid Hormone Nuclear Receptor by Phosphorylation. Methods Mol Biol 1801, 39–46. [PubMed: 29892815]

Liu YY, and Brent GA (2018b). Posttranslational Modification of Thyroid Hormone Nuclear Receptor by Sumoylation. Methods Mol Biol 1801, 47–59. [PubMed: 29892816]

Liu YY, Kogai T, Schultz JJ, Mody K, and Brent GA (2012). Thyroid hormone receptor isoform-specific modification by small ubiquitin-like modifier (SUMO) modulates thyroid hormone-dependent gene regulation. J Biol Chem 287, 36499–36508. [PubMed: 22930759]

Madison DL, Yaciuk P, Kwok RP, and Lundblad JR (2002). Acetylation of the adenovirus-transforming protein E1A determines nuclear localization by disrupting association with importin-α. J Biol Chem 277, 38755–38763. [PubMed: 12161448]

Martin NP, Marron Fernandez de Velasco E, Mizuno F, Scappini EL, Gloss B, Erxleben C, Williams JG, Stapleton HM, Gentile S, and Armstrong DL (2014). A rapid cytoplasmic mechanism for PI3 kinase regulation by the nuclear thyroid hormone receptor, TRβ, and genetic evidence for its role in the maturation of mouse hippocampal synapses in vivo. Endocrinology 155, 3713–3724. [PubMed: 24932806]

Maruvada P, Baumann CT, Hager GL, and Yen PM (2003). Dynamic Shuttling and Intranuclear Mobility of Nuclear Hormone Receptors. Journal of Biological Chemistry 278, 12425–12432. [PubMed: 12506123]

Mavinakere MS, Powers JM, Subramanian KS, Roggero VR, and Allison LA (2012). Multiple novel signals mediate thyroid hormone receptor nuclear import and export. J Biol Chem 287, 31280–31297. [PubMed: 22815488]

Mirza AN, McKellar SA, Urman NM, Brown AS, Hollmig T, Aasi SZ, and Oro AE (2019). LAP2 Proteins Chaperone GLI1 Movement between the Lamina and Chromatin to Regulate Transcription. Cell 176, 198–212 e115. [PubMed: 30503211]

Mondal S, Raja K, Schweizer U, and Mugesh G (2016). Chemistry and Biology in the Biosynthesis and Action of Thyroid Hormones. Angew Chem Int Ed Engl 55, 7606–7630. [PubMed: 27226395]

Mullur R, Liu YY, and Brent GA (2014). Thyroid hormone regulation of metabolism. Physiol Rev 94, 355–382. [PubMed: 24692351]

Nascimento AS, Dias SM, Nunes FM, Aparicio R, Ambrosio AL, Bleicher L, Figueira AC, Santos MA, de Oliveira Neto M, Fischer H, et al. (2006). Structural rearrangements in the thyroid hormone receptor hinge domain and their putative role in the receptor function. J Mol Biol 360, 586–598. [PubMed: 16781732]

Nicoll JB, Gwinn BL, Iwig JS, Garcia PP, Bunn CF, and Allison LA (2003). Compartment-specific phosphorylation of rat thyroid hormone receptor α1 regulates nuclear localization and retention. Mol Cell Endocrinol 205, 65–77. [PubMed: 12890568]

Pawlak M, Lefebvre P, and Staels B (2012). General molecular biology and architecture of nuclear receptors. Curr Top Med Chem 12, 486–504. [PubMed: 22242852]

Rodriguez JA (2014). Interplay between nuclear transport and ubiquitin/SUMO modifications in the regulation of cancer-related proteins. Semin Cancer Biol 27, 11–19. [PubMed: 24704338]

Roggero VR, Zhang J, Parente LE, Doshi Y, Dziedzic RC, McGregor EL, Varjabedian AD, Schad SE, Bondzi C, and Allison LA (2016). Nuclear import of the thyroid hormone receptor α1 is mediated by importin 7, importin β1, and adaptor importin α1. Mol Cell Endocrinol 419, 185–197. [PubMed: 26525414]

Rothenbusch U, Sawatzki M, Chang Y, Caesar S, and Schlenstedt G (2012). Sumoylation regulates Kap114-mediated nuclear transport. EMBO J 31, 2461–2472. [PubMed: 22562154]

Sanchez-Pacheco A, Martinez-Iglesias O, Mendez-Pertuz M, and Aranda A (2009). Residues K128, 132, and 134 in the thyroid hormone receptor-α are essential for receptor acetylation and activity. Endocrinology 150, 5143–5152. [PubMed: 19819978]

Schaaf MJ, Lewis-Tuffin LJ, and Cidlowski JA (2005). Ligand-selective targeting of the glucocorticoid receptor to nuclear subdomains is associated with decreased receptor mobility. Mol Endocrinol 19, 1501–1515. [PubMed: 15705660]

Schaaf MJ, Willetts L, Hayes BP, Maschera B, Stylianou E, and Farrow SN (2006). The relationship between intranuclear mobility of the NF-kappaB subunit p65 and its DNA binding affinity. J Biol Chem 281, 22409–22420. [PubMed: 16760470]

Song EH, Oh W, Ulu A, Carr HS, Zuo Y, and Frost JA (2015). Acetylation of the RhoA GEF Net1A controls its subcellular localization and activity. J Cell Sci 128, 913–922. [PubMed: 25588829]

Soniat M, Cagatay T, and Chook YM (2016). Recognition Elements in the Histone H3 and H4 Tails for Seven Different Importins. J Biol Chem 291, 21171–21183. [PubMed: 27528606]

Soutoglou E, Katrakili N, and Talianidis I (2000). Acetylation regulates transcription factor activity at multiple levels. Mol Cell 5, 745–751. [PubMed: 10882110]

Spilianakis C, Papamatheakis J, and Kretsovali A (2000). Acetylation by PCAF enhances CIITA nuclear accumulation and transactivation of major histocompatibility complex class II genes. Mol Cell Biol 20, 8489–8498. [PubMed: 11046145]

Subramanian KS, Dziedzic RC, Nelson HN, Stern ME, Roggero VR, Bondzi C, and Allison LA (2015). Multiple exportins influence thyroid hormone receptor localization. Mol Cell Endocrinol 411, 86–96. [PubMed: 25911113]

Suh JH, Sieglaff DH, Zhang A, Xia X, Cvoro A, Winnier GE, and Webb P (2013). SIRT1 is a direct coactivator of thyroid hormone receptor β1 with gene-specific actions. PLoS One 8, e70097. [PubMed: 23922917]

Tanida T, Matsuda KI, Yamada S, Hashimoto T, and Kawata M (2015). Estrogen-related Receptor beta Reduces the Subnuclear Mobility of Estrogen Receptor α and Suppresses Estrogen-dependent Cellular Function. J Biol Chem 290, 12332–12345. [PubMed: 25805499]

Thomas M, Dadgar N, Aphale A, Harrell JM, Kunkel R, Pratt WB, and Lieberman AP (2004). Androgen receptor acetylation site mutations cause trafficking defects, misfolding, and aggregation similar to expanded glutamine tracts. J Biol Chem 279, 8389–8395. [PubMed: 14670946]

Wadosky KM, Berthiaume JM, Tang W, Zungu M, Portman MA, Gerdes AM, and Willis MS (2016). MuRF1 mono-ubiquitinates TRalpha to inhibit T3-induced cardiac hypertrophy in vivo. J Mol Endocrinol 56, 273–290. [PubMed: 26862156]

Wang C, Fu M, Angeletti RH, Siconolfi-Baez L, Reutens AT, Albanese C, Lisanti MP, Katzenellenbogen BS, Kato S, Hopp T, et al. (2001). Direct acetylation of the estrogen receptor α hinge region by p300 regulates transactivation and hormone sensitivity. J Biol Chem 276, 18375–18383. [PubMed: 11279135]

Wang C, Tian L, Popov VM, and Pestell RG (2011). Acetylation and nuclear receptor action. J Steroid Biochem Mol Biol 123, 91–100. [PubMed: 21167281]

Weinert BT, Narita T, Satpathy S, Srinivasan B, Hansen BK, Scholz C, Hamilton WB, Zucconi BE, Wang WW, Liu WR, et al. (2018). Time-Resolved Analysis Reveals Rapid Dynamics and Broad Scope of the CBP/p300 Acetylome. Cell 174, 231–244 e212. [PubMed: 29804834]

Weiss M (2004). Challenges and artifacts in quantitative photobleaching experiments. Traffic 5, 662–671. [PubMed: 15296491]

Weitzel JM (2016). Impaired Repressor Function in SUMOylation-Defective Thyroid Hormone Receptor Isoforms. Eur Thyroid J 5, 152–163. [PubMed: 27843805]

Xu Q, Liu X, Zhu S, Hu X, Niu H, Zhang X, Zhu D, Nesa EU, Tian K, and Yuan H (2018). Hyper-acetylation contributes to the sensitivity of chemo-resistant prostate cancer cells to histone deacetylase inhibitor Trichostatin A. J Cell Mol Med 22, 1909–1922. [PubMed: 29327812]

Yang J, Kohler K, Davis DM, and Burroughs NJ (2010). An improved strip FRAP method for estimating diffusion coefficients: correcting for the degree of photobleaching. J Microsc 238, 240–253. [PubMed: 20579262]

Zhang J, Roggero VR, and Allison LA (2018). Nuclear Import and Export of the Thyroid Hormone Receptor. Vitam Horm 106, 45–66. [PubMed: 29407444]

Zhao WX, Tian M, Zhao BX, Li GD, Liu B, Zhan YY, Chen HZ, and Wu Q (2007). Orphan receptor TR3 attenuates the p300-induced acetylation of retinoid X receptor-α. Mol Endocrinol 21, 2877–2889. [PubMed: 17761950]

- The thyroid hormone receptor (TR) undergoes nucleocytoplasmic shuttling.
- We examine the impact of acetylation on localization and intranuclear dynamics.
- Coimmunoprecipitation, FRAP, and transcription assays were performed in cells.
- Nonacetylation mimics show reduced gene transactivation and intranuclear mobility.
- Acetylation mimics show enhanced gene transactivation and cytosolic localization.

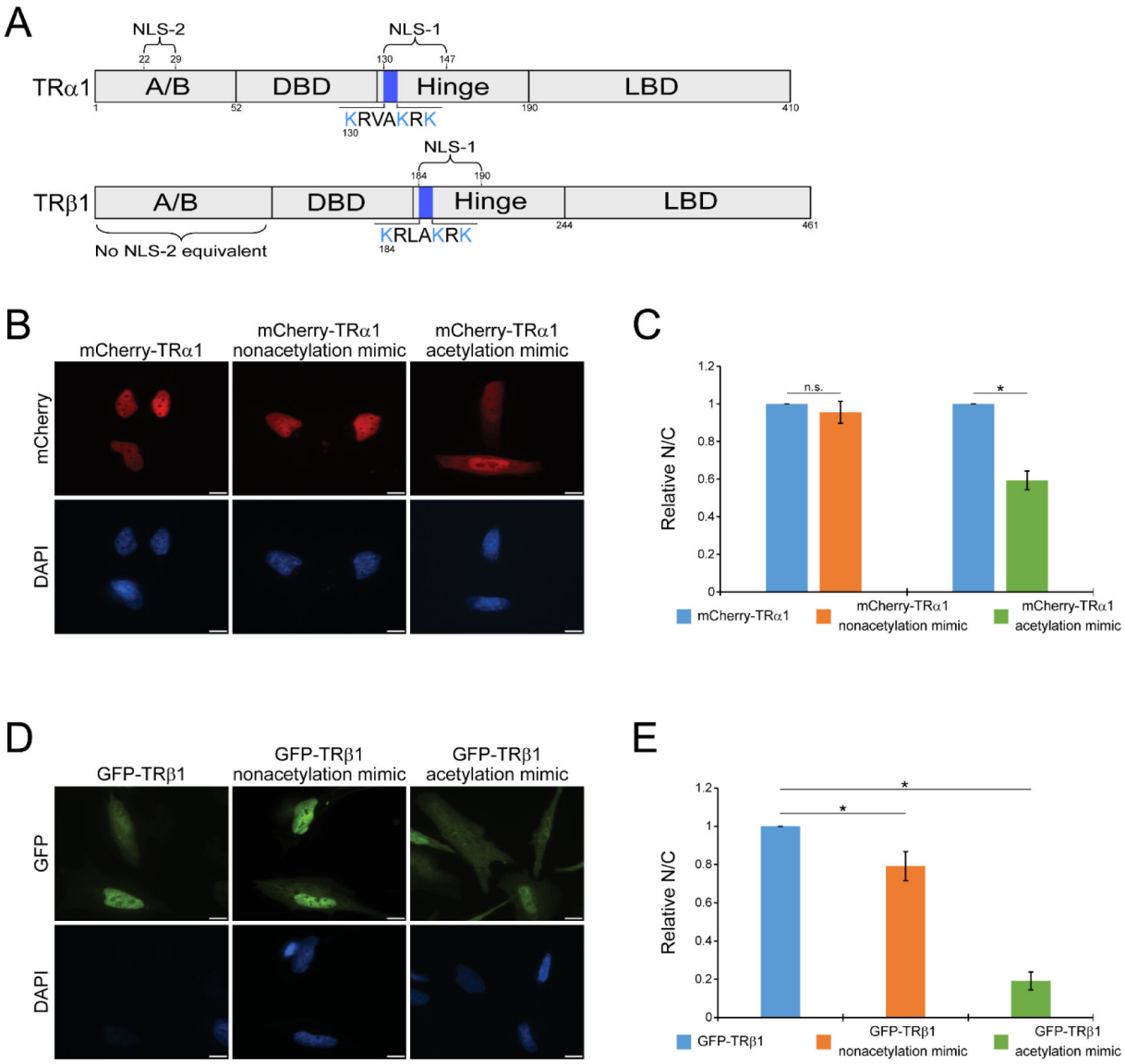

Fig. 1.

Substitution mutations within NLS-1 that mimic acetylation alter TRα1 and TRβ1 intracellular localization. (A) TRα1 and TRβ1 functional domains and acetylation sites. (B) HeLa cells transfected with mCherry-TRα1 and mCherry-TRα1-nonacetylation or acetylation mimic expression plasmids, as indicated, were analyzed by quantitative fluorescence microscopy after fixation and staining with DAPI to visualize the nucleus. Scale bar = 10 μm. (C) Bars indicate the relative N/C for mutant TRα1, normalized to the N/C ratio of wild-type. (D) HeLa cells transfected with GFP-TRβ1 and GFP-TRβ1-nonacetylation or acetylation mimic expression plasmids, as indicated. (E) Bars indicate the relative N/C for mutant TRβ1, normalized to the N/C ratio of wild-type. Error bars indicate ±SEM. (n=3 independent, biologically separate replicate experiments, with 100 cells per replicate). $*P \leq 0.05$, n.s., $P > 0.05$.

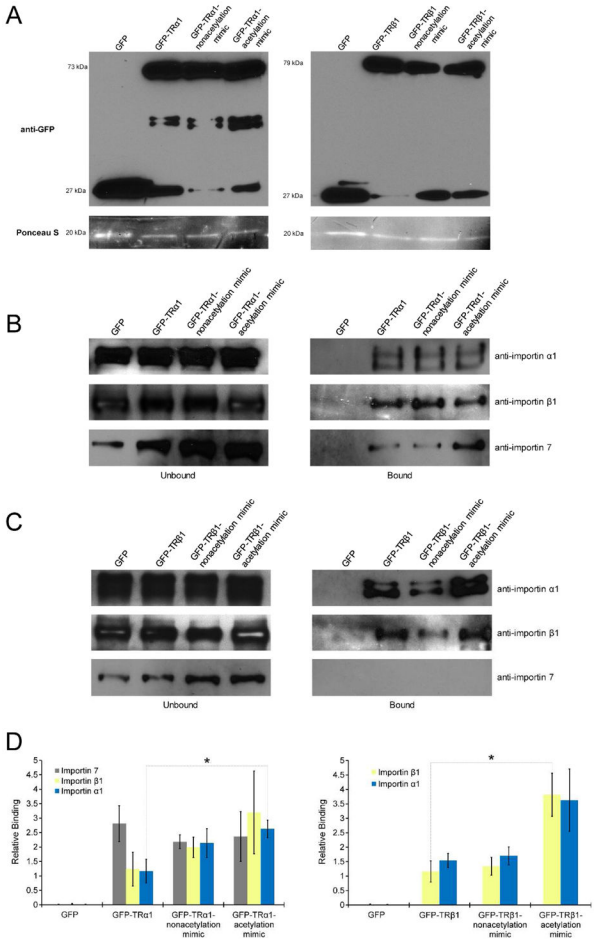

Fig. 2.

TRα1 and TRβ1 acetylation and nonacetylation mimics retain importin binding capability. HeLa cells were transfected with expression plasmids encoding GFP (27 kDa), GFP-TRα1, GFP-TRα1-acetylation or nonacetylation mimic (73 kDa), GFP-TRβ1, GFP-TRβ1-acetylation or nonacetylation mimic (79 kDa), as indicated. Cell lysates were subjected to coimmunoprecipitation using immobilized anti-GFP-antibodies. Representative immunoblots are shown. Protein size was verified using Pre-stained Kaleidoscope protein standards. (A) Trapped GFP-tagged proteins were analyzed by immunoblotting with antibodies specific for GFP. The two lower molecular weight bands in the GFP-TRα1, GFP-TRα1-nonacetylation/acetylation mimic lanes represent specific degradation products. An approximately 20 kDa band revealed by Ponceau S staining was used as an internal control for quantification by densitometry. (B) Immunosupernatants (Unbound) and immunoprecipitates (Bound) from GFP, GFP-TRα1, GFP-TRα1-acetylation or nonacetylation mimic-expressing, and (C) GFP, GFP-TRβ1, GFP-TRβ1-acetylation or nonacetylation mimic-expressing were analyzed on separate immunoblots, with importin-specific antibodies to detect importin 7 (119 kDa), importin β1 (97 kDa), and importin α1 (58 kDa), as indicated. Blots of “unbound” importins appear overexposed relative to “bound” importins, since only a small fraction of each importin in the HeLa cell lysate interacts with TR. (D) Densitometric quantification of “bound” immunoblots relative to the

20 kDa Ponceau S-stained band (see part A). Error bars indicate ± SEM (n=3 independent, biologically separate replicate immunoblots).

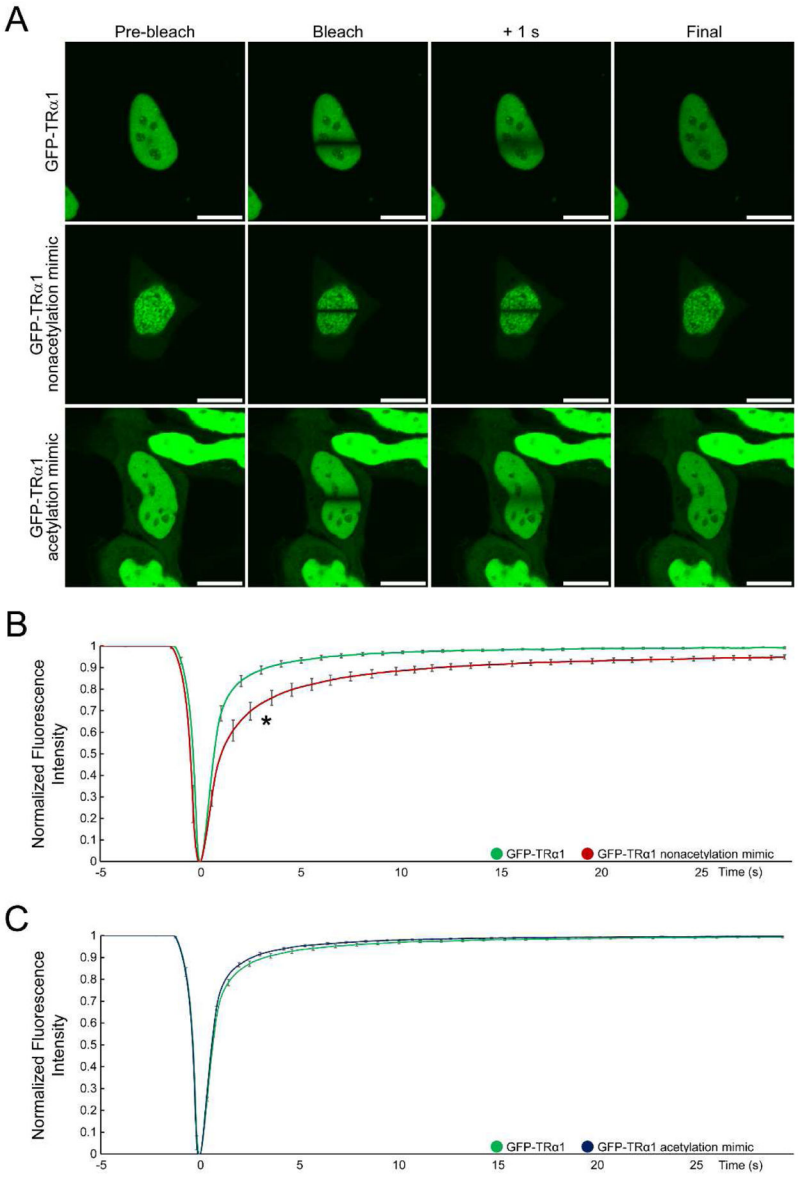

Fig. 3.

The GFP-TRα1 nonacetylation mimic has reduced intranuclear mobility. (A) HeLa cells were transfected with an expression plasmid encoding GFP-TRα1 and its corresponding acetylation and nonacetylation mimics, as indicated. Strip-FRAP was conducted on nuclei from 20 separate cells using a stimulation bleaching line near the middle of the nuclei. Representative images are shown for a nucleus prior to bleach (Pre-bleach), directly after bleaching was terminated (Bleach), 1 s post-bleach (+1 s), and at the end of the recovery period (Final). Scale bar = 10μm. (B) and (C) FRAP curves compare normalized fluorescence intensity over time for TRα1 wild-type and nonacetylation and acetylation mimics, as indicated. Error bars indicate ±SEM (n=3 biologically separate replicates, 20 nuclei per replicate). *P ≤ 0.05.

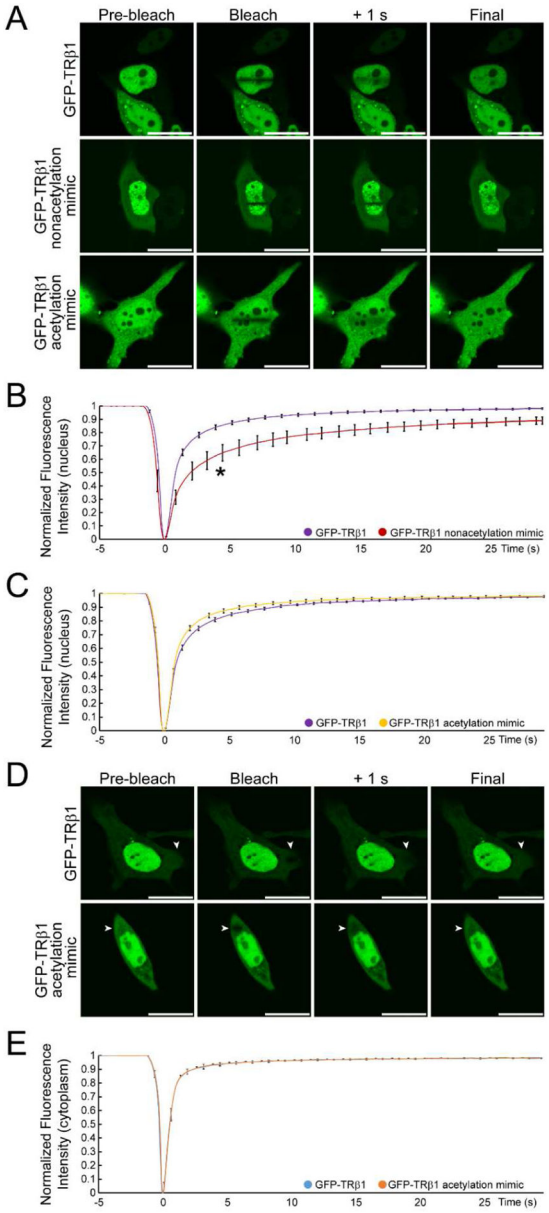

Fig. 4.

The GFP-TRβ1 nonacetylation mimic has reduced intranuclear mobility. (A) HeLa cells were transfected with an expression plasmid encoding GFP-TRβ1 and its corresponding acetylation and nonacetylation mimics, as indicated. Strip-FRAP was conducted on nuclei from 20 separate cells using a stimulation bleaching line near the middle of each nucleus. Representative images are shown for a nucleus prior to bleach (Pre-bleach), directly after bleaching was terminated (Bleach), 1 s post-bleach (+1 s), and at the end of the recovery period (Final). Scale bar = 10μm. (B) and (C) FRAP curves compare normalized fluorescence intensity over time for TRβ1 wild-type and nonacetylation and acetylation mimics, as indicated. Error bars indicate ±SEM (n=3 biologically separate replicates, 20 nuclei per replicate). *$P \leq 0.05$. (D) Representative images of strip-FRAP using a stimulation bleaching line in the cytosol (white arrowheads) of cells expressing GFP-TRβ1

or the GFP-TRβ1 acetylation mimic. (E) FRAP curves for cytosolic mobility. Error bars indicate ±SEM (n=3 biologically separate replicates, 20 nuclei per replicate).

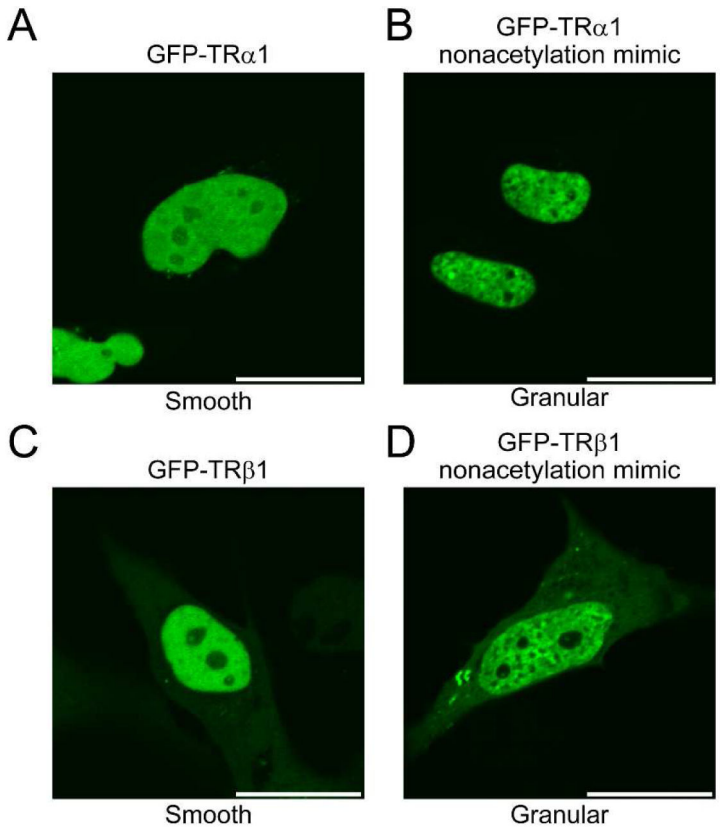

Fig. 5.

TRα1 and TRβ1 wild-type and nonacetylation mimics have a granular nuclear distribution. HeLa cells were transfected with expression plasmids encoding GFP-TRα1, GFP-TRβ1, and their corresponding nonacetylation mimics, as indicated, and live cells were analyzed by confocal microscopy. (A, C) Representative examples of the smooth distribution pattern of wild-type TR. (B, D) Representative examples of the granular, mottled appearance of the GFP-TR nonacetylation mimics. Scale bar = 10 μm.

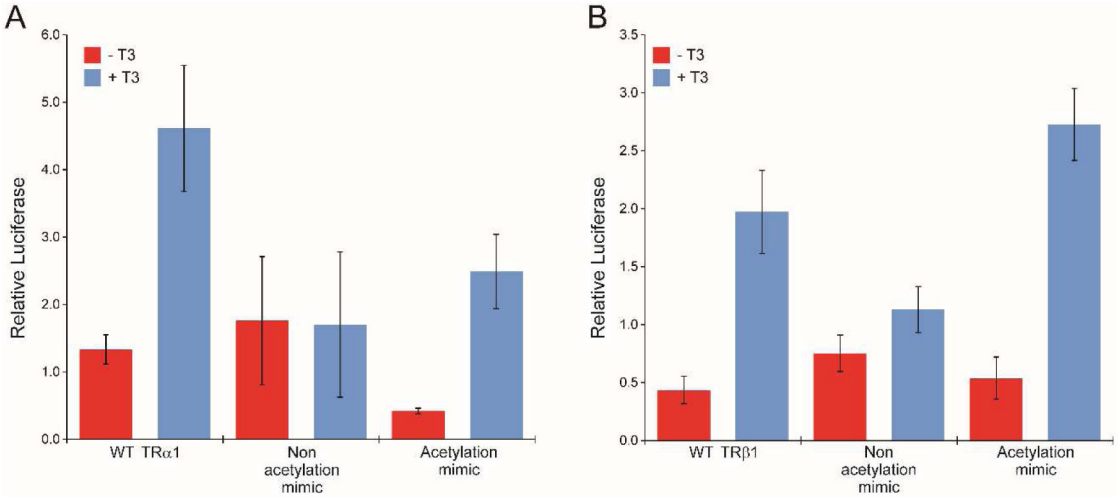

Fig. 6.

Acetylation alters TR-mediated T3-dependent reporter gene transactivation. (A) HeLa cells were cotransfected with expression plasmids for wild-type (WT) GFP-TRα1 and the nonacetylation and acetylation mimics, as indicated, TRE (DR+4)-firefly luciferase reporter, and *Renilla* luciferase internal control, in the presence or absence of T3. Data are presented as relative firefly/*Renilla* luciferase activity (Relative Luciferase). Error bars indicate ± SEM (n = 4 biologically independent replicates of 8 wells per treatment). (B) Parallel experiments with GFP-TRβ1.

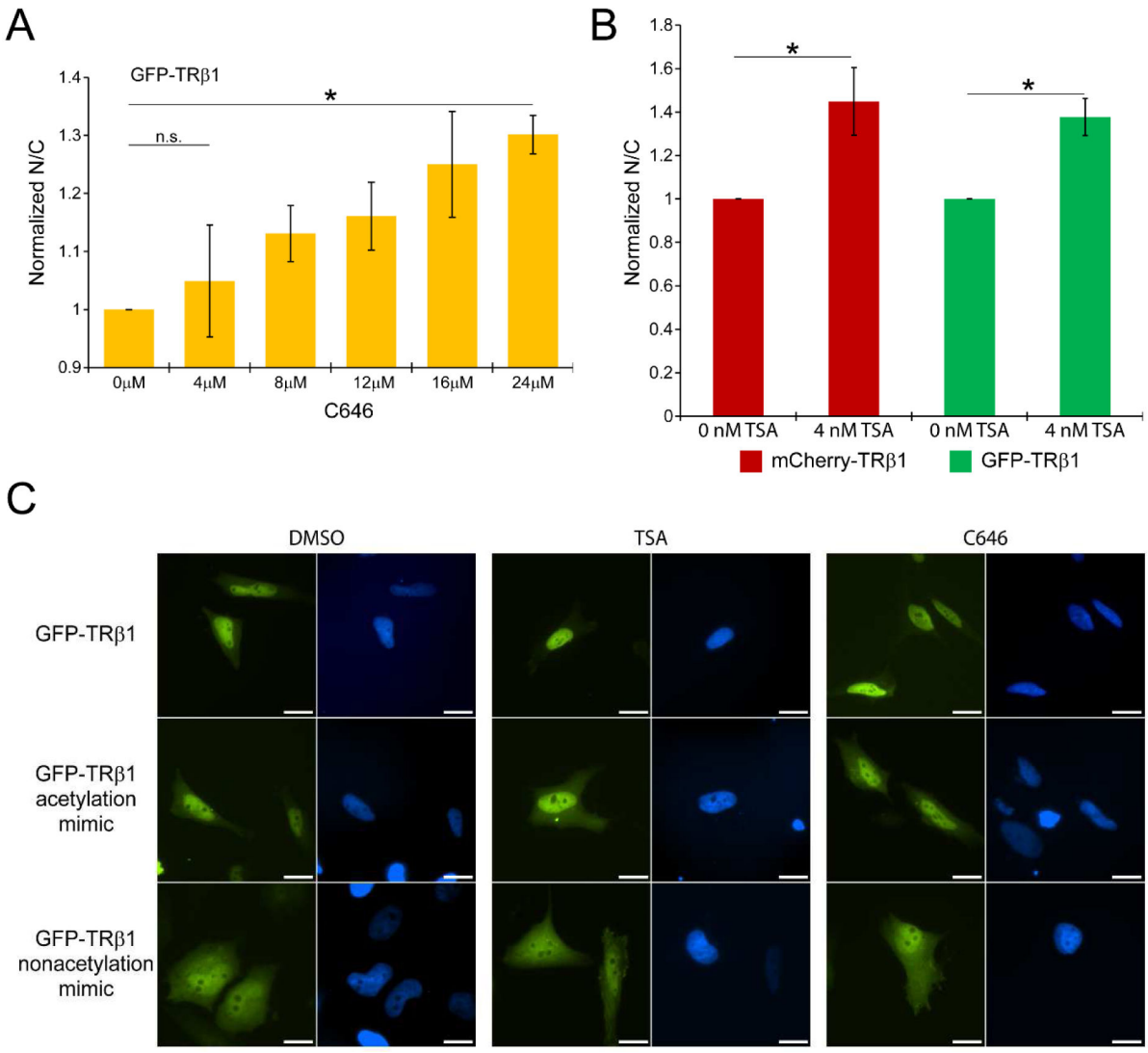

Fig. 7.

Inhibition of the acetyltransferase CBP/p300 by C646 promotes wild-type TRβ1 nuclear retention. (A) Fluorescence microscopy was used to analyze the N/C for GFP-TRβ1 in transfected HeLa cells, as described in Fig. 1. Bars indicate N/C for TRβ1-expressing cells treated with increasing dosages of C646, a CBP/p300-specific acetyltransferase inhibitor, normalized to cells treated with the vehicle DMSO (0 μM). (B) HeLa cells were transfected with GFP-TRβ1 or mCherry-TRβ1 expression plasmids and treated with 4 nM TSA, a general deacetylase inhibitor. Bars indicate N/C for TRβ1-expressing cells, normalized to cells treated with vehicle (0 nM TSA). n=3 independent, biologically separate replicate experiments, with 100 cells per replicate. Error bars indicate ± SEM. *$P \leq 0.05$; n.s., $P > 0.05$. (C) Representative images of HeLa cells transfected with GFP-TRβ1 wild-type, acetylation mimic and nonacetylation mimic expression plasmids, treated with DMSO (vehicle), 16 μM C646, or 4 nM TSA, as indicated. Scale bar = 10 μm.

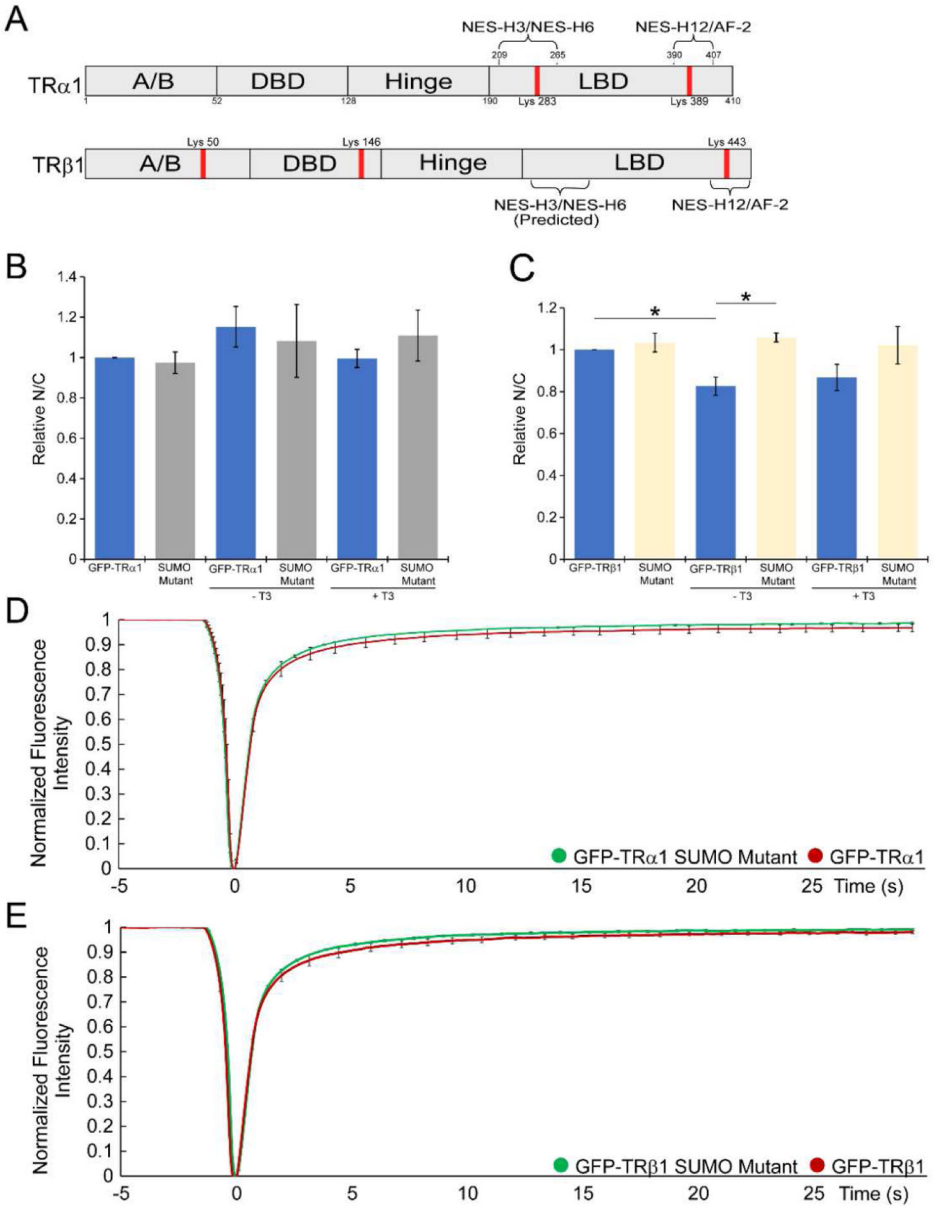

Fig. 8.

Sumoylation-deficient mutants of TR display wild-type nuclear localization and intranuclear dynamics. (A) The domain structure of TRα1 and TRβ1 (not to scale) showing sumoylation sites. TRα1 is sumoylated at K283 and 389 in the LBD between the two NESs. The sumoylation sites for TRβ1 are located at K50, 146, and 443 in the A/B domain, DBD, and LBD (Liu et al., 2012). (B and C) HeLa cells were transfected with GFP-TRα1 wild-type or sumoylation-deficient expression plasmids, or GFP-TRβ1 wild-type or sumoylation-deficient expression plasmids, as indicated, in the presence of standard medium (MEM/10% FBS) or in MEM supplemented with charcoal-stripped FBS in the presence (+T3) or absence of T3 (-T3). Fixed cells were analyzed by quantitative fluorescence microscopy for the intracellular distribution pattern of the fluorescent fusion proteins. Bars indicate relative N/C, normalized to N/C for cells in standard medium. Error bars indicate ±SEM. n = 3

biologically separate replicates, 100 cells per replicate. *P<0.05. (D) FRAP curves comparing wild-type and sumoylation-deficient TRα1. Strip-FRAP was performed as described in Fig. 3. (E) FRAP curves comparing wild-type and sumoylation-deficient TRβ1.

Table 1

Intranuclear FRAP profiles for GFP-TRα1, GFP-TRβ1, and the acetylation and nonacetylation mimics.

TR Subtype	Recovery Rate	Mobile Fraction	Immobile Fraction	Half-time slope	t½ (s)
TRα1 (control)	0.008 ± 0.000	0.993 ± 0.006	0.007 ± 0.006	0.831 ± 0.031	0.628 ± 0.039
TRα1-acetylation mimic	0.007 ± 0.000	0.997 ± 0.004	0.003 ± 0.003	0.913 ± 0.038	0.561 ± 0.038
	P = 0.106	*P* = 0.313	*P* = 0.313	*P* = 0.046	*P* = 0.100
TRα1 (control)	0.008 ± 0.001	0.993 ± 0.006	0.007 ± 0.006	0.802 ± 0.094	0.673 ± 0.067
TRα1-nonacetylation mimic	0.012 ± 0.002	0.949 ± 0.018	0.051 ± 0.018	0.536 ± 0.140	1.009 ± 0.242
	P = 0.042	*P* = 0.014	*P* = 0.014	*P* = 0.053	*P* = 0.080
TRβ1 (control)	0.012 ± 0.001	0.980 ± 0.008	0.025 ± 0.008	0.604 ± 0.044	0.875 ± 0.067
TRβ1-acetylation mimic	0.010 ± 0.001	0.980 ± 0.010	0.019 ± 0.010	0.674 ± 0.054	0.785 ± 0.078
	P = 0.047	*P* = 0.542	*P* = 0.542	*P* = 0.154	*P* = 0.203
TRβ1 (control)	0.010 ± 0.001	0.980 ± 0.011	0.020 ± 0.011	0.660 ± 0.069	0.819 ± 0.099
TRβ1-nonacetylation mimic	0.015 ± 0.003	0.889 ± 0.061	0.111 ± 0.061	0.336 ± 0.203	1.817 ± 0.901
	P = 0.007	*P* = 0.005	*P* = 0.005	*P* = 0.004	*P* = 0.022
TRβ1 (cytosol, control)	0.006± 0.001	0.980 ± 0.003	0.020 ± 0.003	1.075 ± 0.216	0.516 ± 0.103
TRβ1-acetylation mimic (cytosol)	0.006± 0.001	0.984 ± 0.002	0.016 ± 0.002	1.045 ± 0.199	0.516 ± 0.102
	P = 0.877	*P* = 0.105	*P* = 0.105	*P* = 0.869	*P* = 1.000
TRα1 (control)	0.008± 0.001	0.965 ± 0.027	0.035 ± 0.027	0.780 ± 0.077	0.673 ± 0.068
Sumoylation-deficient TRα1	0.008± 0.000	0.986 ± 0.005	0.014 ± 0.005	0.811 ± 0.052	0.651 ± 0.039
	P = 0.886	*P* = 0.260	*P* = 0.260	*P* = 0.593	*P* = 0.650
TRβ1 (control)	0.008± 0.001	0.977 ± 0.012	0.022 ± 0.012	0.817 ± 0.068	0.650 ± 0.039
Sumoylation-deficient TRβ1	0.008± 0.000	0.990± 0.006	0.010 ± 0.006	0.803 ± 0.025	0.673 ± 0.000
	P = 0.761	*P* = 0.195	*P* = 0.191	*P* = 0.738	*P* = 0.374